Fabrication of β-Ga_2O_3/Si heterointerface and characterization of interfacial structures for high-power device applications

Jianbo Liang[1]*, Daiki Takatsuki[1], Masataka Higashiwaki[2], Yasuo Shimizu[3], Yutaka Ohno[4], Yasuyoshi Nagai[3], and Naoteru Shigekawa[1]

[1]*Electronic Information Systems, Osaka City University, 3-3-138 Sumiyoshi, Osaka 558-8585, Japan*

[2]*National Institute of Information and Communications Technology, 4-2-1 Nukui-Kitamachi, Koganei, Tokyo 184-8795, Japan.*

[3]*Institute for Materials Research (IMR), Tohoku University, 2145-2 Narita, Oarai, Ibaraki 311-1313, Japan*

[4]*Institute for Materials Research (IMR), Tohoku University, 2-1-1 Katahira, Sendai 980-8577, Japan*

E-mail: liang@osaka-cu.ac.jp

In this work, we fabricated Ga_2O_3(001)/Si(100) and Ga_2O_3(010)/Si(100) heterointerfaces by surface-activated bonding (SAB) at room temperature and investigated the effect of Si thickness on the thermal stability of the heterointerfaces by heating the bonding samples at different temperatures. The heterointerface with a thin Si exhibited a good thermal stability at 1000 ℃. A 4-nm-thick intermediate layer with a uniform thickness was formed at the as-bonded Ga_2O_3(001)/Si(100) heterointerface, but for the as-bonded Ga_2O_3(010)/Si(100) heterointerface, an intermediate layer with a non-uniform thickness was formed. The thickness of both intermediate layers ranged from 3.6 to 5.4 nm and decreased after annealing at 500 ℃, followed by an increase after annealing at 1000 ℃. The component of the intermediate layer includes Ga, O, and Si atoms.

1. Introduction

Beta-phase single crystal gallium oxide (β-Ga_2O_3) is a new type of semiconductor material with a bandgap of 4.8 eV and the high breakdown electric field of 8 MV/cm.[1–4] Baliga's figure of merit for Ga_2O_3 is several times higher than that for silicon carbide (SiC) or gallium nitride (GaN).[5] It is also one of the most promising candidates for the next-generation semiconductor material required by high-power device applications. High-quality β-Ga_2O_3 can be grown by the Bernoulli,[6] floating zone (FZ),[7] Czochralski,[8,9] and edge-defined film-fed growth (EFG) processes.[10] Furthermore, 4-inch Ga_2O_3 wafers grown by EFG are already commercially available. Since the growth rate of the EFG process is very high (up to 15 mm/h), Ga_2O_3 has a significant advantage in terms of production cost compared to other wide-band-gap semiconductor materials such as SiC, GaN, aluminum nitride (AlN), and diamond.[11] Ga_2O_3 as a transparent substrate applied to ultraviolet (UV) optical detectors[12] and light-emitting diodes (LEDs)[13] has been reported.

N-type doping of Ga_2O_3 with Si or Sn has shown a good controllability: the doped impurity density can be precisely controlled over the wide range of 10^{16} to 10^{20} cm^{-3}.[14–16] There are currently active research and development efforts on the application of n-type Ga_2O_3 to the Schottky barrier diode (SBD),[17,18] metal-semiconductor field-effect transistors (MSFETs),[3,19,20] and metal-oxide-semiconductor field-effect transistors (MOSFETs).[21–23] In contrast to n-type doping Ga_2O_3, p-type doping Ga_2O_3 with high hole conductivity has not yet been possible due to the deep impurity level exhibited in the doping, which makes it very difficult to activate at room temperature. Hence, the lack of an efficient p-type doping β-Ga_2O_3 severely limits the development of Ga_2O_3-based devices with a pn junction. One potential solution is to fabricate a heterojunction using p-type semiconductors other than β-Ga_2O_3. The silicon (Si) semiconductor is the most commonly used semiconductor in the electronics field today thanks to its state-of-the-art device fabrication process technology and low-cost production. If Ga_2O_3 and Si could be combined, it would be possible not only to overcome the bottleneck of Ga_2O_3 doping, but also to integrate Ga_2O_3-based devices and large scale integrated (LSI) SI with various functions on the same substrate.

The direct growth of Ga_2O_3 on Si and vice versa is considered the most promising technique for directly integrating Ga_2O_3 and Si. However, the large differences in their crystal structures and thermal expansion coefficients would make the direct growth very

difficult. Another potential technique is wafer direct bonding technique, which can overcome the lattice structure and thermal expansion mismatches between the integrating materials. Prior research has reported the successful fabrication of p-Si/n-SiC, p-Si/n-GaAs, p-Si/p-InGaAs, p-Si/n-InGaP, and p-Si/p-diamond heterojunctions by the direct wafer bonding method.[24–30] The fabricated heterojunctions show excellent electrical properties and the reverse biased currents of the Si/SiC and Si/diamond heterojunctions have been significantly improved by the post-annealing process. We previously reported the fabrication of a Ga_2O_3/Si heterointerface using surface activated bonding (SAB) and obtained a void-free bonding interface.[31]

In this work, we utilized SAB to fabricate Ga_2O_3(001)/Si(100) and Ga_2O_3(010)/Si(100) heterointerfaces at room temperature. We then measured the thermal stability of their heterointerfaces at 500 and 1000 °C in N_2 gas ambient pressure and investigated the effect of Ga_2O_3 crystal direction on the thermal stability. The interfacial structures and components of the Ga_2O_3(001)/Si(100) and Ga_2O_3(010)/Si(100) heterointerfaces with and without annealing at different temperatures were systematically investigated using transmission electron microscopy (TEM) and energy-dispersive X-ray spectroscopy.

2. Experimental methods

β-Ga_2O_3 (001) and (010), Si (100), and Si semiconductor-on-insulator (SOI) substrates were used for fabricating the Ga_2O_3/Si heterointerfaces. The SOI substrate was composed of a 5-μm-thick Si (100) layer and a 0.3-μm-thick SiO_2 layer formed on a Si substrate. The thicknesses of the Ga_2O_3 (001), Ga_2O_3 (010), and Si (100) substrates were 0.65, 0.50, and 0.52 mm, respectively. The averaged roughness (Ra) of the Ga_2O_3 (001) and (010) surfaces was measured by atomic force microscopy (AFM) to be 0.262 and 0.219 nm, respectively. These substrates were cleaned with acetone and isopropyl alcohol in an ultrasonic bath for 300 s and then dried in a N_2 flow. The cleaned Ga_2O_3 and Si or Ga_2O_3 and SOI substrates were placed inside the SAB equipment, and then activated by Ar fast atom beam (FAB) irradiation in a high vacuum lower than 5×10^{-6} Pa. The current and voltage of the Ar FAB irradiation were 1.62 mA and 1.65 kV, respectively. After irradiation, the substrates were immediately brought into contact by applying a load of 100 MPa at room temperature. Ga_2O_3(001)/Si(100), Ga_2O_3(010)/Si(100), Ga_2O_3(001)/SOI, and Ga_2O_3(010)/SOI

heterointerfaces were then fabricated at room temperature. The Ra value of the irradiated Ga_2O_3 (001) and (010) substrate surfaces were measured to be 0.164 and 0.204 nm, respectively. AFM images of the Ga_2O_3 (001) and (010) substrate surfaces before and after Ar FAB irradiation are shown in Fig. 1(a), (b), and (c), (d), respectively. After bonding, the Si substrates of Ga_2O_3(001)/SOI and Ga_2O_3(010)/SOI bonded samples were removed by mechanical polishing and wet etching processes. The thermal stability test was conducted in a quartz tube furnace at 500 and 1000 ℃ with a heating rate of 45 ℃/min under an ambient of N_2 for 1 min, and cooling was not controlled. The interfacial structure observation and compositional analysis were carried out using TEM and EDS under a scanning transmission electron microscopy (STEM) model with a JEOL JEM-2200FS analytical microscope. The TEM samples were fabricated by a focused ion beam (FIB) technique (Helios Nano Lab600i; Fisher Scientific) at room temperature.

3. Results and discussion

3.1 Results

Figure 2 shows optical microscope images of the (a), (c) as-bonded, (b) 500 ℃-annealed, and (d) 1000 ℃-annealed Ga_2O_3(001)/Si(001) bonded sample surfaces, respectively. A full contact area was observed in the Ga_2O_3(001)/Si as-bonded samples. After annealing at 500 ℃, part of the Ga_2O_3(010) separated from the bonded sample. When the annealing temperature rose to 1000 ℃, cracks were observed in the Ga_2O_3(001) bonded to Si. Figure 3 shows optical microscope images of the (a), (c) as-bonded, (b) 500 ℃-annealed, and (d) 1000 ℃-annealed Ga_2O_3(010)/Si bonded sample surfaces, respectively. As with the Ga_2O_3(001) substrate, a full contact area was observed in the as-bonded Ga_2O_3(010)/Si samples. However, after annealing at 500 ℃, a large part of the bonded interface separated. This separated area was further expanded after annealing at 1000 ℃, and cracks were observed in the annealed sample.

Figure 4(a)–4(c) shows optical microscope images of the as-bonded, 500 ℃-annealed, and 1000 ℃-annealed Si thin film bonded to Ga_2O_3(001) substrate samples. Some areas not covered by Si film were observed in the as-bonded sample due to the mechanical polishing and side etching during the Si substrate removal process. In contrast to the bonded samples of the Ga_2O_3 and Si substrates, no reduction in the bonded area and no cracks were observed

in the bonded samples after annealing at 500 and 1000 ℃. Optical microscope images of the as-bonded, 500 ℃-annealed, and 1000 ℃-annealed Si thin film bonded to Ga_2O_3(010) substrate samples are shown in Fig. 5(a)–(c), respectively. Like the bonded samples of the Si thin film and Ga_2O_3 (001) substrates, no reduction in the bonded area was observed in the Si thin film bonded to Ga_2O_3(010) substrate samples after annealing at 500 and 1000 ℃. Furthermore, no cracks were observed.

Cross-sectional TEM images of the as-bonded, 500 ℃-annealed, and 1000 ℃-annealed Ga_2O_3(001)/Si bonding interfaces are shown in Fig. 6(a)-(c), respectively. An intermediate layer with a uniform thickness (about 4 nm) was observed at the as-bonded interface. After annealing at 500 ℃, the thickness decreased to 1.5 nm, but when the annealing temperature rose to1000 ℃, the thickness increased to 13.2 nm. Figure 7(a)-(c) shows cross-sectional TEM images of the as-bonded, 500 ℃-annealed, and 1000 ℃-annealed Ga_2O_3(010)/Si bonding interfaces, respectively. The intermediate layer was also observed at the as-bonded Ga_2O_3(010)/Si interface but had a non-uniform thickness ranging from 3.6 to 5.4 nm. After annealing at 500 ℃, the thickness slightly decreased to between 2.5 and 4.1 nm, but when the annealing temperature rose to 1000 ℃, the thickness significantly increased, similarly to the 1000 ℃-annealed Ga_2O_3(001)/Si interfaces, and was determined to range between 10.5 and 12.8 nm.

Cross-sectional STEM images and the X-ray intensity profiles for the Ga, O, Si, Ar, and Fe atoms (highlighted in green, red, orange, blue, and dark green, respectively) of the as-bonded, 500 ℃-annealed, and 1000 ℃-annealed Ga_2O_3(001)/Si bonding interfaces are shown in Fig. 8(a)-(c), respectively. A small peak for the intensity profile of the Fe atoms was observed only at the as-bonded Ga_2O_3(001)/Si interface, which seems to have originated from the metal vacuum chamber during the Ar beam irradiation of the bonding process. Prior research using time-of-flight secondary ion mass spectrometry (TOF-SIMS) has shown that Fe atoms exist only on the surface irradiated by Ar beam irradiation,[30] which means the peak position of the relative intensity of Fe atoms should be located on the bonding interface. We observed intensity gradients for the Ga, O, and Si atoms in the intermediate layer. The depth of the Ar beam irradiation damage on the Ga_2O_3(001) substrate was measured to be about 4 nm on the basis of the intensity gradients. After annealing at 500 ℃, Ga and Si atoms diffused into the Si and Ga_2O_3(001) substrates adjacent to the intermediate layer. A small

peak for the intensity profile of the Ar atoms and a Ga transition layer were also observed. We attribute this peak to the concentration of Ar atoms distributed in the intermediate layer. The full width at half maximum (FWHM) of the intensity profile for Fe atoms became larger, and the damage depth of the Ga_2O_3(001) substrate irradiated by the Ar beams was not much improved. After annealing at 1000 ℃, no peaks for the Ar and Fe atoms intensity profiles were observed, and the intensity gradients for the Ga, O, and Si atoms in the intermediate layer became lower than those for the as-bonded and 500 ℃-annealed Ga_2O_3(001)/Si interfaces. We attribute the disappearance of the peak in the intensity profiles of the Fe and Ar atoms to the fact that the concentration of these atoms distributed in the intermediate layer was below the resolution of the detector sensor of the EDS due to diffusion after annealing. The Ga and Si atoms further diffused into the Si and Ga_2O_3(001) substrates adjacent to the intermediate layer when the annealing temperature was increased.

Figure 9(a)-(c) shows cross-sectional STEM images and the X-ray intensity profiles for the Ga, O, Si, Ar, and Fe atoms of the as-bonded, 500 ℃-annealed, and 1000 ℃-annealed Ga_2O_3(010)/Si bonding interfaces, respectively. In contrast to the as-bonded Ga_2O_3(001)/Si interface, no peak for the intensity profile of the Fe atoms was observed at the as-bonded Ga_2O_3(010)/Si interface. We hypothesize that the interface location can be determined by relying on the intensity gradient for the Si atoms adjacent to the Si substrate, as the Si surface was subjected to the same impact by the Ar beam irradiation during bonding. Intensity gradients for the Ga, O, and Si atoms were also observed in the intermediate layer of the as-bonded interface. The depth of the Ar beam irradiation damage on the Ga_2O_3(010) substrate was about 8 nm, which is larger than that of the as-bonded Ga_2O_3(001)/Si interface, and Si atoms diffused into the Ga_2O_3(010) substrate adjacent to the intermediate layer of the as-bonded interface. After annealing at 500 ℃, the depth of the Si atoms diffused into the Ga_2O_3(010) substrate became shallower. The intensity gradients for the Ga, O, and Si atoms became more abrupt in the intermediate layer. When the annealing temperature rose to 1000 ℃, the interdiffusion of Ga, O, and Si near the bonding interface made the intensity gradient lowest in the intermediate layer.

3.2 Discussion

Peeling of the bonding interface and substrate cracks were observed in the bonded sample of Ga_2O_3 and Si substrates after annealing at high temperature, while no peeling or cracks were observed in the bonded sample of the Si thin film and Ga_2O_3 substrates. The thermal expansion coefficient of Ga_2O_3 (001) ($6.34 \times 10^{-6}/K$) and (010) ($7.8 \times 10^{-6}/K$) substrates is known to be more than two times higher than that of Si (100) ($2.62 \times 10^{-6}/K$).[33,34] A large thermal stress tends to generate in the Ga_2O_3/Si interface at high temperature, and this stress is further increased in the interface with both thick substrates, which results in peeling or cracks in the bonded substrate. On the other hand, the thermal stress generated by the thermal expansion coefficient mismatch between Ga_2O_3 and Si is smaller in the interface with a Si thin film, where the thermal stress normal to the thin film is typically released. When a stress works along the bonding interface, another stress with an opposite sign will be generated in the direction perpendicular to the bonding interface due to the Poisson's ratio. In the case of thin films, stress perpendicular to the thin film is released due to the influence of the surface, resulting in a decrease of stress along the bonding interface. Similar results have been reported in GaAs/diamond,[35] InGaP/diamond,[36] and GaN/diamond[37] heterointerfaces.

The observed intensity gradients for Ga, O, and Si atoms indicate that the intermediate layer formed at the interface was an atomic intermixing layer composed mainly of Ga, O, and Si atoms. The thickness reduction of the atomic intermixing layer after annealing at 500 ℃ suggests that the atomic intermixing layer thickness can be controlled by the post-annealing process. However, we found that after annealing at 1000 ℃, the thickness of the atomic intermixing layer was significantly increased. This behavior differs from that in the directly bonded GaAs/InP,[38] Si/diamond,[39] and Si/SiC[24] heterointerfaces, in which the thickness of the atomic intermixing layer disappeared after annealing at an optimum temperature. We speculate that the annealing temperature of 1000 ℃ might be too high for the Ga_2O_3 substrate. Such a high temperature accelerates the interdiffusion of the atoms near the interface, forming Si dioxide that would reach a thermal equilibrium state at elevated temperatures in the Si-oxygen binary system.[40] An optimal annealing temperature somewhere between 500 and 1000 ℃ is thus required for removing the damage on the Ga_2O_3 substrate caused by the Ar beam irradiation. We found that the thickness uniformity of the intermediate layer formed at the interface and the damage of the Ar beam irradiation

on the Ga_2O_3 surface were different depending on the Ga_2O_3 substrate-plane orientation. In addition, although no significant difference was observed in the Ra value of the Ga_2O_3 (001) and (010) surfaces irradiated by the Ar beam, bamboo shoot-shaped objects were observed in the AFM image of the irradiated Ga_2O_3 (010) surface (as shown in Fig. 1(d)). These results indicate that the Ar beam irradiation has a large impact on the Ga_2O_3 (010) substrate surface, which seems to be related to the atomic density of the Ga_2O_3 substrate-plane orientation. The atomic densities of the Ga_2O_3 (010) and (001) planes were calculated to be 2.9×10^{15} and $3.77 \times 10^{15}\ cm^{-2}$, respectively, by referring to the lattice constant and crystal structure of Ga_2O_3.[41)]

4. Conclusion

In this study, we fabricated Ga_2O_3(001)/Si(100) and Ga_2O_3(010)/Si(100) heterointerfaces through the direct bonding of Si and Ga_2O_3 using the SAB technique at room temperature. The bonded sample with a thin Si exhibited a better thermal stability at 1000 ℃ compared to the sample with a thick Si. An intermediate layer with a uniform thickness was formed at the as-bonded Ga_2O_3(001)/Si(100) interface, while the intermediate layer formed at the as-bonded Ga_2O_3(010)/Si(100) interface was non-uniform in thickness. Furthermore, the layer formed at the as-bonded Ga_2O_3(001)/Si(100) interface was thinner than that of the as-bonded Ga_2O_3(010)/Si(100) interface. The thickness of the intermediate layer decreased after annealing at 500 ℃, and significantly increased after annealing at 1000 ℃. The intermediate layer was a mixed layer composed of Ga, O, and Si atoms. The damage caused by Ar-beam irradiation to the Ga_2O_3(010) surface was greater than that to the Ga_2O_3(001) surface. These results demonstrate that thin Si film bonded to a Ga_2O_3 substrate can withstand the harsh device fabrication process, and that the intermediate layer formed at the interface can be removed by optimizing the post-annealing process.

Acknowledgments

This work was supported by JSPS KAKENHI Grant Numbers: 19H02182. The fabrication of the TEM samples was performed at The Oarai Center and at the Laboratory of Alpha-Ray Emitters in IMR under the Inter-University Cooperative Research in IMR of Tohoku

University (NO. 20M0030). A part of this work was supported by Kyoto University Nano Technology Hub in the "Nanotechnology Platform Project" sponsored by the Ministry of Education, Culture, Sports, Science and Technology (MEXT), Japan.

References

1) H. H. Tippins, Phys. Rev. **140**, A316 (1965).
2) M. Orita, H. Ohta, M. Hirano, and H. Hosono, Appl. Phys. Lett. **77**, 4166 (2000).
3) M. Higasiwaki, K. Sasaki, A. Kuramata, T. Masui, and S. Yamakoshi, Appl. Phys. Lett. **100**, 013504 (2012).
4) K. Sasaki, A. Kuramata, T. Masui, E. G. Víllora, K. Shimamura, and S. Yamakoshi, Appl. Phys. Express **5**, 035502 (2012).
5) M. Higasiwaki, H. Murakami, Y. Kumagai, and A. Kuramata, Jpn. J. Appl. Phys. **55**, 1202A1 (2016).
6) M. Fleischer and H. Meixner, J. Appl. Phys. **74**, 300 (1993).
7) N. Ueda, H. Hosono, R. Waseda, and H. Kawazoe, Appl. Phys. Lett. **70**, 3561 (1997).
8) Z. Galazka, R. Uecker, K. Irmscher, M. Albrecht, D. Klimm, M. Pietsch, M. Brutzam, R. Bertram, S. Ganschow, and R. Fornari, Cryst. Res. Technol. **45**, 1229 (2010).
9) Z. Galazka, K. Irmscher, R. Uecker, R. Bertram, M. Pietsch, A. Kwasniewski, M. Naumann, T. Schulz, R. Schewski, D. Klimm, and M. Bickermann, J. Gryst. Growth **404**, 184 (2014).
10) H. Aida, K. Nishiguchi, H. Takeda, N. Aota, K. Sunakawa, and Y. Yaguchi, Jpn. J. Appl. Phys. **47**, 8506 (2008).
11) A. Kuramata, K. Koshi, S. Watanabe, Y. Yamaoka, T. Masui, and S. Yamakoshi, Jpn. J. Appl. Phys. **55**, 1202A2 (2016).
12) T. Oshima, T. Okuno, N. Arai, N. Suzuki, S. Orita, and S. Fujita, Appl. Phys. Express **1**, 011202 (2008).
13) K. Shimamura, E. G. Villora, K. Domen, K. Yui, K. Aoki, and N. Ichinose, Jpn. J. Appl. Phys. **44**, L7 (2005).
14) T. Onuma, S. Fujioka, T. Yamaguchi, M. Higashiwaki, K. Sasaki, T. Masui, and T. Honda,

Appl. Phys. Lett. **103**, 041910 (2013).

15) E. G. Víllora, K. Shimamura, Y. Yoshikawa, T. Ujiie, and K. Aoki, Appl. Phys. Lett. **92**, 202120 (2008).
16) N. Suzuki, S. Ohira, M. Tanaka, T. Sugawar, K. Nakajima, and T. Shishido, Phys. Status Solidi C **4**, 2310 (2007).
17) K. Sasaki, M. Higashiwaki, A. Kuramata, T. Masui, and S. Yamakoshi, IEEE Electron Device Lett. **34**, 493 (2013).
18) Q. He, W. Mu, H. Dong, S. Long, Z. Jia, H. Lv, Q. Liu, M. Tang, X. Tao, and M. Liu, Appl. Phys. Lett. **110**, 093503 (2017).
19) J. Bae, H. Kim, I. H. Kang, and J. Lim, J. Mater. Chem. C, **8**, 2687 (2020).
20) J. Ma, H. Cho, J. Heo, S. Kim, G. Yoo, Adv. Elect. Mater. **5**, 1800938 (2019).
21) M. Higashiwaki, K. Sasaki, T. Kamimura, M. H. Wong, D. Krishnamurthy, A. Kuramata, T. Masui, and S. Yamakoshi, Appl. Phys. Lett. **103**, 123511 (2013).
22) Z. Feng, Y. Cai, Z. Li, Z. Hu, Y. Zhang, X. Lu, X. Kang, J. Ning, C. Zhang, Q. Feng, J. Zhang, H. Zhou, and Y. Hao, Appl. Phys. Lett. **116**, 243503 (2020).
23) K. Sasaki, M. Higashiwaki, A. Kuramata, T. Masui, and S. Yamakoshi, Appl. Phys. Express **6**, 086502 (2013).
24) J. Liang, S. Nishida, M. Arai, and N. Shigekawa, Appl. Phys. Lett. **104**, 161604 (2014).
25) S. Nishida, J. Liang, M. Morimoto, N. Shigekawa, and M. Arai, Mater. Sci. Forum **778-780**, 718 (2014).
26) J. Liang, S. Nishida, M. Arai, and N. Shigekawa, J. Appl. Phys. **120**, 034504 (2016).
27) J. Liang, T. Miyazaki, M. Morimoto, S. Nishida, N. Watanabe, and N. Shigekawa, Appl. Phys. Express **6**, 021801 (2013).
28) J. Liang, M. Morimoto, S. Nishida, and N. Shigekawa, Phys. Status Solidi C **10**, 1644 (2013).
29) K. S. Mckay, F. P. Lu, J. Kim, C. Yi, A. S. Brown, and A. R. Hawkins, Appl. Phys. Lett. **90**, 222111 (2007).
30) Y. Uehigashi, S. Ohmagai, H. Umezawa, H. Yamada, J. Liang, and N. Shigekawa, Diamond Relat. Mater. **120**, 108665 (2021).
31) J. Liang, D. Takatsuki, Y. Shimizu, M. Higashiwaki, Y. Ohno, Y. Nagai, and N. Shigekawa, Proc. 7th Int. IEEE Workshop Low-Temperature Bonding for 3D Integration,

2021, p. 19.

32) Y. Ohno, J. Liang, N. Shigekawa, H. Yoshida, S. Takeda, R. Miyagawa, Y. Shimizu, and Y. Nagai, Appl. Sur. Sci. **525**, 146610 (2020).
33) M. E. Liao, C. Li, H. M. Yu, E. Roshker, M. J. Tadjer, K. D. Hobart, and M. S. Coorsky, Appl. Phys. Lett. Mater. **7**, 022517 (2019).
34) Y. Okada and Y. Tokumaru, J. Appl. Phys. **56**, 314 (1984).
35) J. Liang, Y. Nakamura, T. Zhan, Y. Ohno, Y. Shimizu, K. Katayama, T. Watanabe, H. Yoshida, Y. Nagai, H. Wang, M. Kasu, N. Shigekawa, Diamond Relat. Mater. **111**, 108207 (2021).
36) J. Liang, Y. Nakamura, Y. Ohno, Y. Shimizu, Y. Nagai, H. Wang, N. Shigekawa, Funct. Diamond **1**, 110 (2021).
37) J. Liang, A. Kobayashi, Y. Shimizu, Y. Ohno, S.-W, Kim, K. Koyama, M. Kasu, Y. Nagai, and N. Shigekawa, Adv. Mater. **33**, 2104564 (2021).
38) H. Wada, Y. Ogawa, and T. Kamijoh, Appl. Phys. Lett. **62**, 738 (1993).
39) J. Liang, S. Masuya, S. Kim, T. Oishi, M. Kasu, and N. Shigekawa, Appl. Phys. Express **12**, 016501 (2019).
40) T. B. Massalski, H. Okamoto, P. R. Subramanian, Binary Alloy Phase Diagrams (Materials Park, Ohio: ASM International, 1990) 2nd ed., p. 2915.
41) Z. Cheng, M. Hanke, Z. Galazka, and A. Trampert, Appl. Phys. Lett. **113**, 182102 (2018).

Figure Captions

Fig. 1. AFM images of Ga_2O_3(001) and (010) surfaces (a), (c) before and (b), (d) after Ar FAB irradiation.

Fig. 2. Optical microscope images of (a), (c) as-bonded, (b) 500 ℃-annealed, and (d)

1000 ℃-annealed Ga_2O_3(001)/Si bonded samples.

Fig. 3. Optical microscope images of (a), (c) as-bonded, (b) 500 ℃-annealed, and (d) 1000 ℃-annealed Ga_2O_3(010)/Si bonded samples.

Fig. 4. Optical microscope images of (a) as-bonded, (b) 500 ℃-annealed, and (c) 1000 ℃-annealed Si thin film bonded to Ga_2O_3(001) substrate samples.

Fig. 5. Optical microscope images of (a) as-bonded, (b) 500 ℃-annealed, and (c) 1000 ℃-annealed (c) Si thin film bonded to Ga_2O_3(010) substrate samples.

Fig. 6. Cross-sectional TEM images of (a) as-bonded, (b) 500 ℃-annealed, and (c) 1000 ℃-annealed Ga_2O_3(001)/Si bonding interfaces.

Fig. 7. Cross-sectional TEM images of (a) as-bonded, (b) 500 ℃-annealed, and (c) 1000 ℃-annealed (c) Ga_2O_3(010)/Si bonding interfaces.

Fig. 8. Cross-sectional STEM images and X-ray intensity profiles for Ga, O, Si, Ar, and Fe atoms (green, red, orange, blue, and dark green, respectively) of (a) as-bonded, (b) 500 ℃-annealed, and (c) 1000 ℃-annealed Ga_2O_3(001)/Si bonding interfaces.

Fig. 9. Cross-sectional STEM images and X-ray intensity profiles for Ga, O, Si, Ar, and Fe atoms (green, red, orange, blue, and dark green, respectively) of (a) as-bonded, (b) 500 ℃-annealed, and (c) 1000 ℃-annealed Ga_2O_3(010)/Si bonding interfaces.

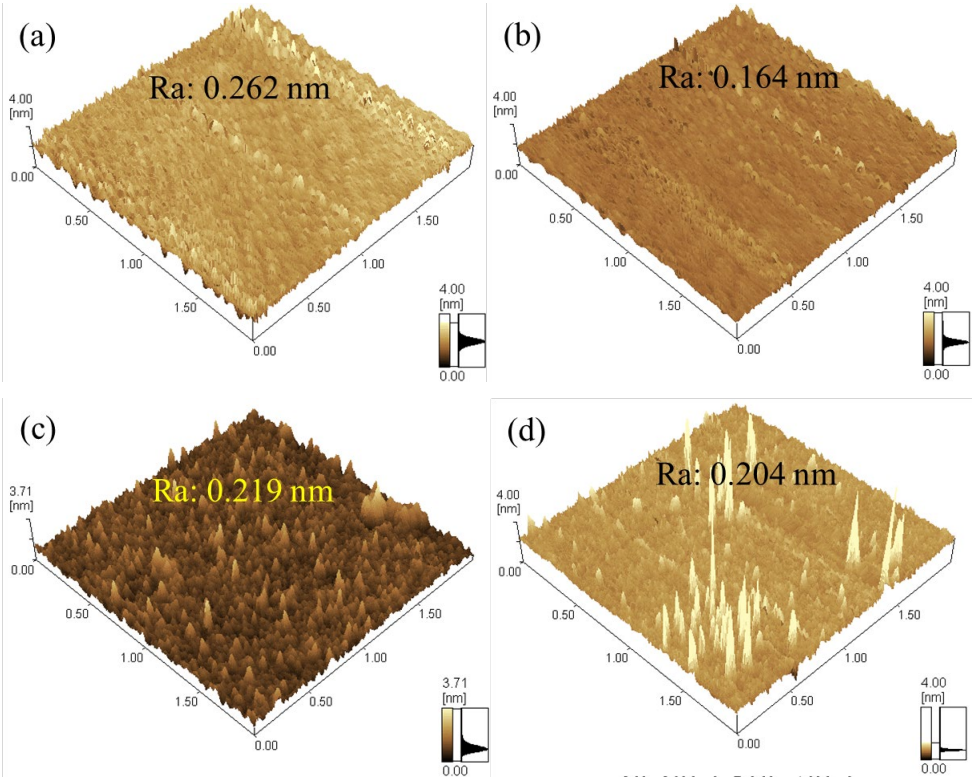
(a)
Ra: 0.262 nm
(b)
Ra: 0.164 nm
(c)
Ra: 0.219 nm
(d)
Ra: 0.204 nm

Fig.1.

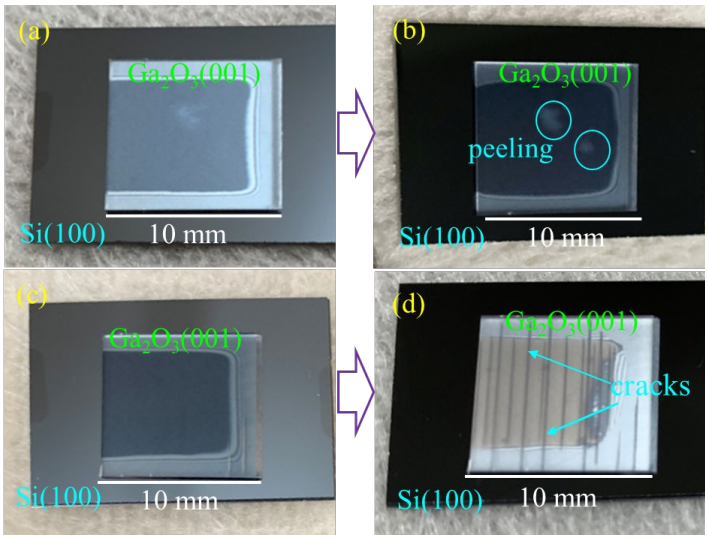
(a)
Ga2O3(001)
Si(100)
10 mm
(b)
Ga2O3(001)
peeling
Si(100)
10 mm
(c)
Ga2O3(001)
Si(100)
10 mm
(d)
Ga2O3(001)
cracks
Si(100)
10 mm

Fig. 2.

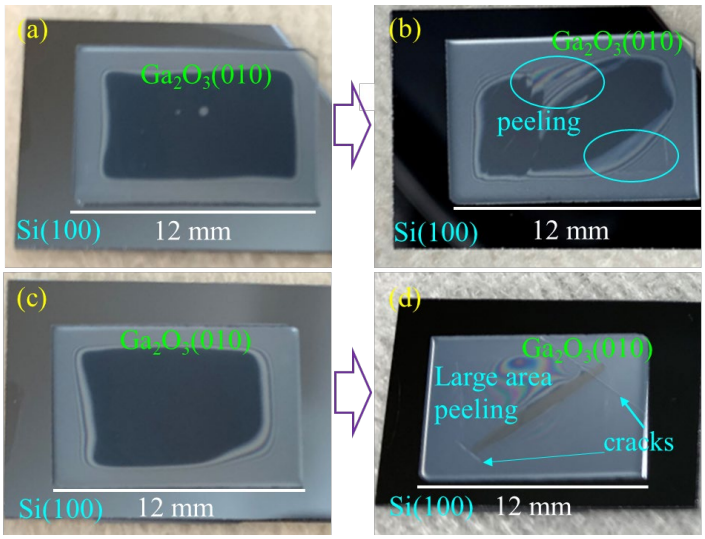

Fig. 3.

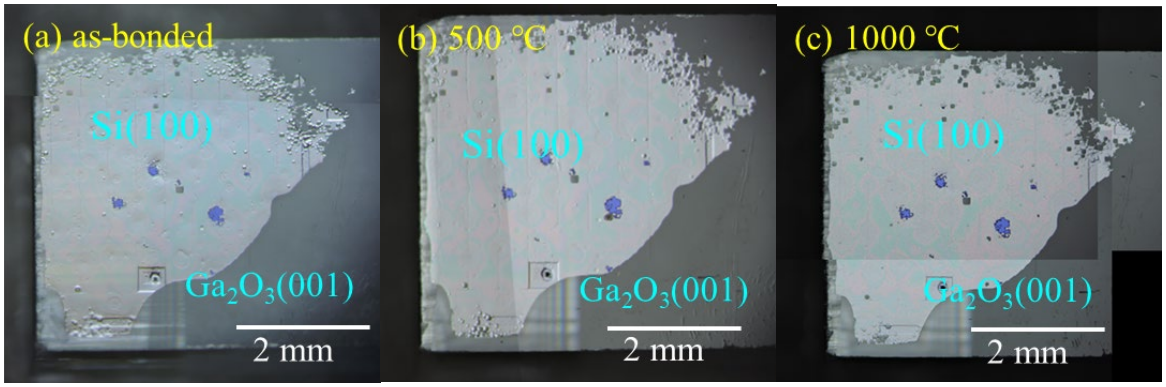

Fig. 4.

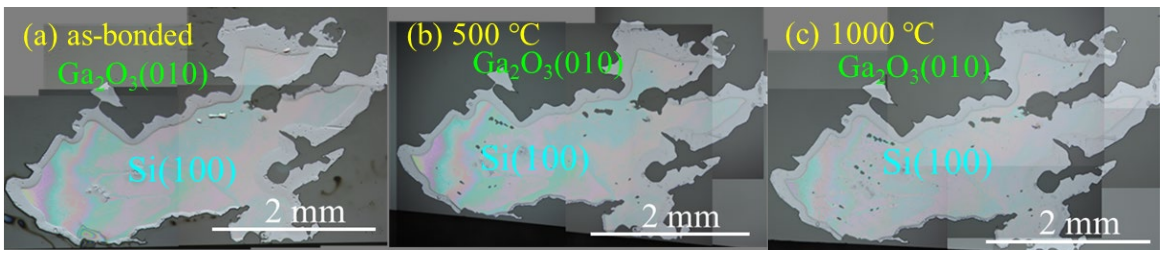

Fig. 5.

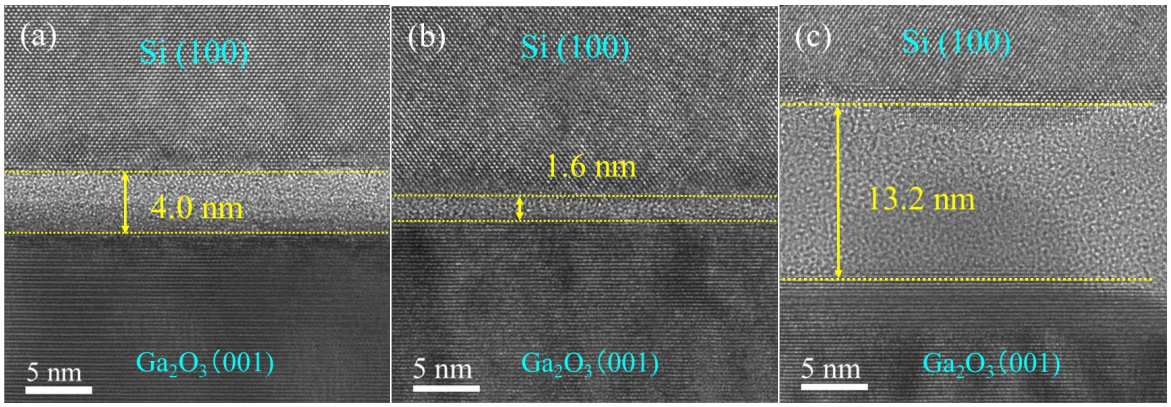

Fig. 6.

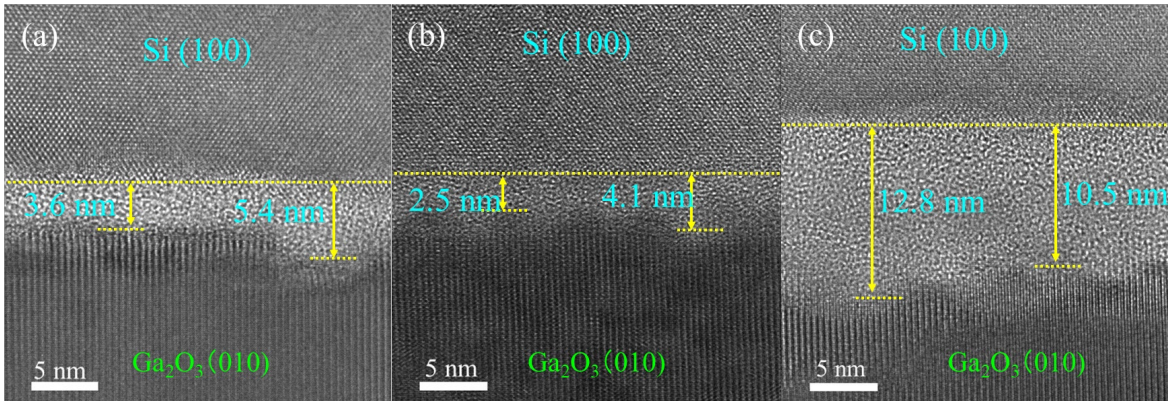

Fig. 7.

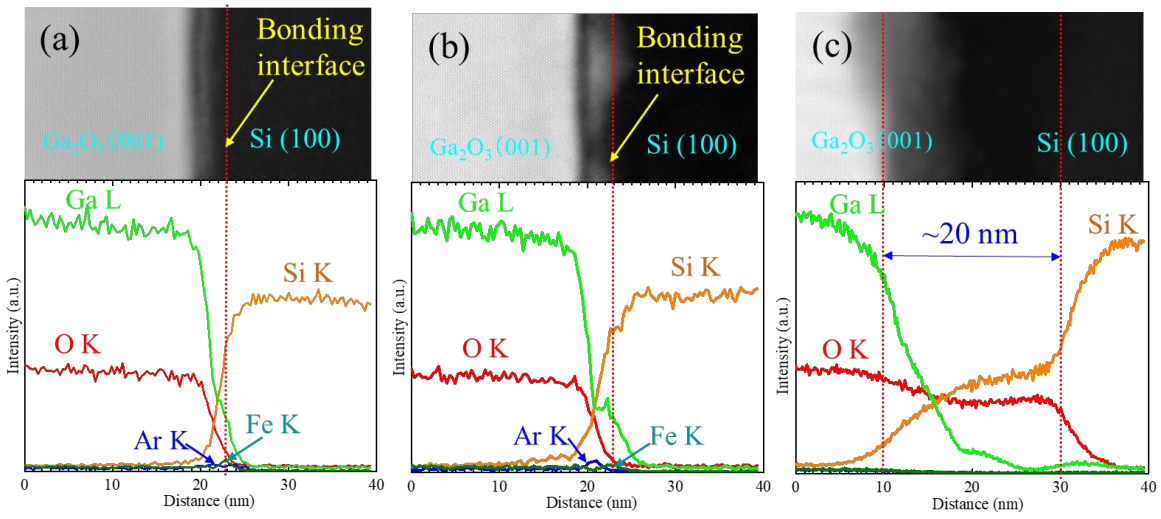

Fig. 8.

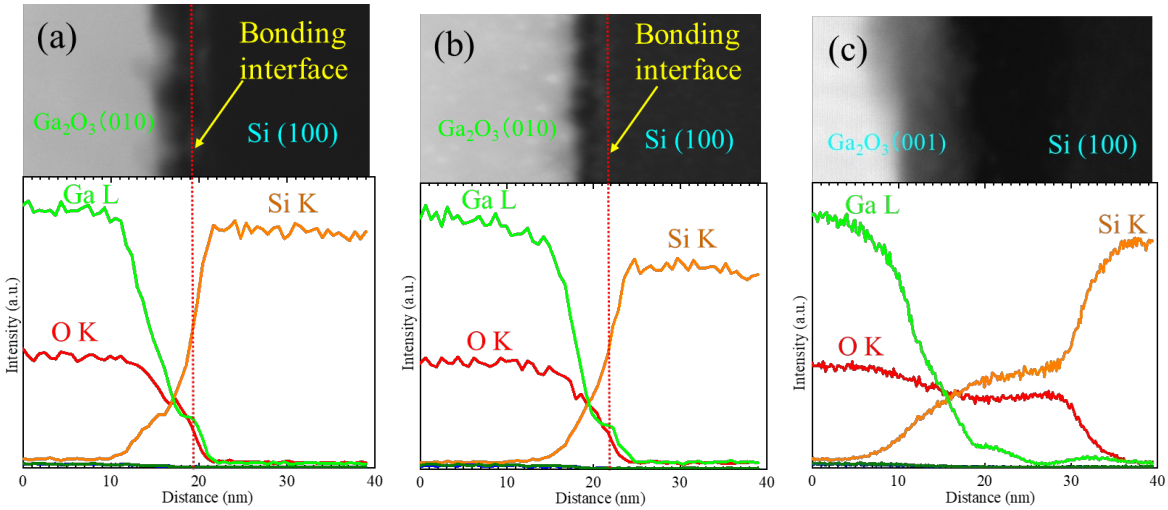
(a)
Bonding interface
Ga2O3 (010)
Si (100)
Ga L
Si K
O K
Intensity (a.u.)
0
10
20
30
40
Distance (nm)
(b)
Bonding interface
Ga2O3 (010)
Si (100)
Ga L
Si K
O K
Intensity (a.u.)
0
10
20
30
40
Distance (nm)
(c)
Ga2O3 (001)
Si (100)
Ga L
Si K
O K
Intensity (a.u.)
0
10
20
30
40
Distance (nm)

Fig. 9.